

Quantum Teleportation Coexisting with Conventional Classical Communications in Optical Fiber

JORDAN M. THOMAS^{1,*}, FEI I. YEH², JIM HAO CHEN², JOE J. MAMBRETTI², SCOTT J. KOHLERT³, GREGORY S. KANTER^{1,4}, AND PREM KUMAR^{1,5}

¹Center for Photonic Communication and Computing, Northwestern University, 2145 Sheridan Road, Evanston, IL 60208, USA

²International Center for Advanced Internet Research, Northwestern University, 750 N. Lake Shore Drive, Chicago, IL 60611, USA

³Ciena Corporation, 7035 Ridge Road, Hanover, MD 21076, USA

⁴NuCrypt, LLC, 1460 Renaissance Drive, Suite #205, Park Ridge, IL 60068, USA

⁵Department of Physics and Astronomy, Northwestern University, 2145 Sheridan Road, Evanston, IL 60208-3112, USA

*jordanthomas2025@u.northwestern.edu

Compiled May 17, 2024

The ability for quantum and classical networks to operate in the same optical fibers would aid the deployment of quantum network technology. However, quantum performance can be susceptible to noise photons generated by spontaneous Raman scattering of high-power coexisting classical light. Quantum teleportation is a fundamental operation in quantum networking, but has yet to be demonstrated in fibers populated with high data rate conventional optical signals. In this paper, we demonstrate a three-node quantum state teleportation system coexisting with 400-Gbps C-band classical communications in 30.2 km of fiber. To protect quantum fidelity, Raman noise rates are suppressed using optimized O-band quantum channels and filtering in multiple degrees of freedom. Fidelity is shown to be well maintained with elevated classical powers as high as 18.7 dBm, which could support multiple classical channels with many terabits/s aggregate data rates. These results show the feasibility of advanced quantum and classical network applications operating within a unified fiber infrastructure.

<http://dx.doi.org/10.1364/ao.XX.XXXXXX>

1. INTRODUCTION

The optical fiber infrastructure and telecommunications technology that underlie the Internet have been widely adopted by researchers seeking to develop quantum networks capable of applications such as quantum-enhanced cryptography, sensing, and networked quantum computing [1, 2]. However, since the majority of the existing fiber infrastructure is populated with classical network signals, whether or not quantum networking can be realized on a large scale will depend on the ability for both quantum and classical networks to operate in the same fibers due to limited existing fiber connections and the high cost of new installation.

Quantum and classical signals can readily share a single fiber via standard wavelength division multiplexing. However, inelastic scattering of high-power classical light can generate noise photons that obscure the detection of typically sub-photon-level quantum signals. Spontaneous Raman scattering (SPRS) is most prominent due to its broadband spectrum that spans the telecom bands. Without careful design, classical signals require significant attenuation to perform quantum operations, resulting in a trade-off between achievable classical data rates or quantum fidelity.

Quantum-classical integration has been studied for various systems, such as weak coherent states (WCSs) [3–12], entangled photon pairs [13–22], Bell state measurements (BSMs) on WCSs [23, 24], continuous variables [25], and squeezed light [26]. However, many systems that are integral to future quantum network architectures, such as those utilizing quantum teleportation, remain unexplored. Using the non-local properties of entanglement, quantum teleportation enables the transfer of a quantum state between two distant physical systems without direct transmission of the systems themselves [27]. It plays a foundational role in advanced applications such as quantum relays [28], quantum repeaters [29], networking quantum computers [30], and other applications in quantum science and technology [31].

Recent years have seen impressive progress towards implementing teleportation-based systems in quantum-dedicated fiber networks [31–37], but teleportation over fibers carrying conventional classical communications signals has yet to be demonstrated. The ability to perform teleportation alongside modern classical networking without sacrificing fidelity would be an important step in ensuring advanced quantum networks can make full use of the existing fiber infrastructure.

In this paper, we demonstrate a three-node quantum state

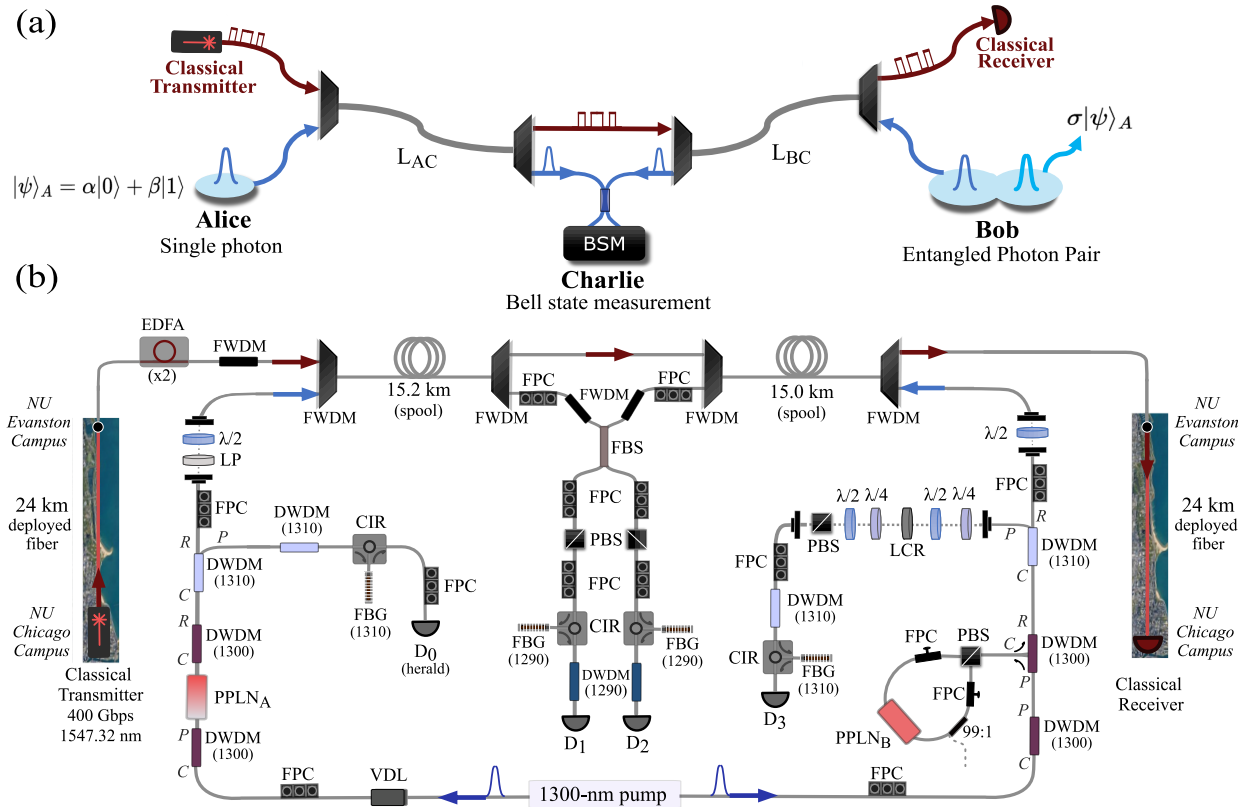


Fig. 1. (a) Conceptual diagram of the experiment. Alice prepares a qubit $|\psi\rangle_A$ that she wishes to transfer onto one photon of an entangled Bell state photon pair at Bob via quantum teleportation. Alice encodes $|\psi\rangle_A$ onto a single photon, which is multiplexed into a fiber of length L_{AC} to co-propagate with a high-rate classical communications signal to a node at Charlie. The classical signal by-passes Charlie's node to continue propagating over a fiber of length L_{BC} . Two photons are prepared in an entangled Bell state at Bob's node. One photon counter-propagates with the classical signal over this fiber to Charlie to undergo a Bell state measurement (BSM) with Alice's qubit. After a BSM detection, Alice's state is destroyed whilst the other entangled photon at Bob's node is projected onto the state $\sigma|\psi\rangle_A$, where σ is a unitary transformation unique to the BSM result. (b) Experimental implementation. Quantum and classical signals coexist in 30.2 km of fiber ($L_{AC} = 15.2$ km, $L_{BC} = 15.0$ km). Alice and Bob both generate photon pairs with wavelengths of 1290 nm and 1310 nm via non-degenerate spontaneous parametric down-conversion. Alice's source heralds a single photon, whereas Bob prepares a two-photon entangled state. Qubits are encoded in polarization and the 1290-nm photons from each source are transmitted to Charlie for the BSM. The classical signal has a rate of 400-Gbps and is allocated to the 1547.32 nm C-band wavelength channel. This signal travels an additional 24-km of deployed fiber before and after multiplexing, giving a total classical link distance of 78.2 km (FPC = fiber polarization controller, DWDM = dense wavelength division multiplexer, FWDM = O-band/C-band WDM, PPLN = periodically poled lithium niobate waveguide, $\lambda/2$ = half-wave plate, $\lambda/4$ = quarter-wave plate, LP = linear polarizer, LCR = liquid crystal retarder, PBS = polarizing beam splitter, FBS = 50:50 fiber coupler, VDL = variable optical delay line, FBG = fiber Bragg grating, CIR = circulator, D_j = superconducting nanowire single photon detector, C = common port, P = pass port, R = reflect port, EDFA = erbium doped fiber amplifier).

teleportation system operating over 30.2 km of optical fiber that simultaneously carries high-power C-band classical communications at a rate of 400 Gbps. Teleportation is performed via a joint BSM on a single photon and one member of an entangled Bell state photon pair [38]. Utilizing wavelength multiplexing of quantum and classical signals, a heralded single photon carrying a polarization encoded qubit and one photon of an entangled Bell state photon pair are distributed over roughly 15 km of fiber to undergo a BSM near the midpoint of the fiber, whilst classical light traverses the full 30.2 km link plus an additional 48 km of deployed fiber.

We implement multiple techniques to minimize the degradation of quantum fidelity by SpRS noise. At the quantum source nodes, we generate and distribute photons with O-band wave-

lengths < 1300 nm. Due to the multi-mode SpRS spectrum, these are the telecom wavelengths with nearly the minimum SpRS photon generation probability from the C-band classical source [17]. At quantum receiver nodes, we employ narrow-band spectral filtering and coincidence detection temporal filtering to reject uncorrelated in-band noise photons. This combines various approaches used in high-power quantum-classical coexistence studies of WCSs [9–12], entangled photons [17], and BSMs on two WCSs [24], but has not been investigated in the context of quantum teleportation.

We first demonstrate that our system's exceptionally low noise rates allow for no significant impact on entanglement distribution to the BSM nor Hong-Ou-Mandel (HOM) interference [39] between independent photons, which are the underlying op-

erations of the photonic quantum teleportation protocol [38]. We then perform quantum state teleportation, where we measure an average state transfer fidelity of $89.8 \pm 3.1\%$ with elevated classical C-band powers as high as 74 mW (18.7 dBm) launched into the fiber link. We discuss methods to improve both raw teleportation fidelity and noise-resilience as well as the implications of our results for future quantum networking.

This experiment demonstrates approaches for integrating many key classical and quantum network components, including high-rate C-band classical signals and optical amplifiers, single photon and entangled photon pair distribution, and multi-qubit operations such as BSMs all operating simultaneously in the same fibers.

2. EXPERIMENTAL DESIGN

A conceptual diagram of the experiment is shown in Fig. 1(a). Alice generates a single photon to encode the quantum state $|\psi\rangle_A = \alpha|0\rangle + \beta|1\rangle$ that she wishes to teleport to Bob. Alice's photon is multiplexed into an optical fiber of length L_{AC} to co-propagate with a classical communications signal to a BSM node at Charlie. The classical signal is de-multiplexed just prior to the BSM and then re-multiplexed to bypass Charlie's node. The classical signal then travels along another fiber of length L_{BC} , counter-propagating with respect to one photon from an entangled Bell state photon pair generated at Bob's node. During the BSM at Charlie, both photons are irreversibly destroyed by the detection whilst Bob's other photon of the entangled pair is projected onto the state $|\psi\rangle_B = \sigma|\psi\rangle_A$, where σ is a unitary operation that is unique to the BSM result and can be classically communicated to Bob to reconstruct Alice's state [27].

Fig. 1(b) shows the physical realization of the experiment. In our case, Alice's state is encoded onto a heralded single photon's polarization, L_{AC} is 15.2 km, and L_{BC} is 15.0 km. Thus, the quantum state transfer distance, and the distance in which quantum and classical signals coexist, is 30.2 km.

The classical source consists of a 400-Gbps C-band transceiver operating at 1547.32 nm (Ciena WaveLogic 5 Nano 400ZR). To reduce the amount of SpRS noise photons that are generated into the quantum channels, we strategically place our quantum signals in the O-band so that they have an anti-Stokes frequency detuning from the C-band as well as suppressed Raman gain at the far offset detuning between the C- and O-bands [4]. Instead of the commonly used 1310-nm wavelength allocation [9–12, 24], our transmitted quantum signals are at a wavelength of 1290 nm. This channel has roughly an order of magnitude lower SpRS noise due to the non-uniform SpRS spectrum across the O-band [17], resulting in a higher tolerance to C-band power.

Alice and Bob generate their respective quantum signals via type-0 cascaded second harmonic generation-spontaneous parametric down conversion (c-SHG-SPDC) photon pair generation [40]. Alice and Bob both have independent periodically-poled lithium niobate (PPLN) waveguides that are each phase matched for SHG at 650 nm, which pumps the SPDC process to generate a two-mode squeezed vacuum state with a non-degenerate joint spectrum centered around 1300 nm. This state approximates a single photon pair given the probability of generating a pair per mode is $\ll 1$. The cascaded second order nonlinear process is analogous to four-wave mixing, which we pump using a 1300-nm distributed feedback laser that is intensity modulated using a lithium niobate modulator to generate pulses with an approximate 65-ps temporal full-width at half maximum (FWHM) and a repetition rate of 500 MHz. This pump is then split and directed

to Alice and Bob's nodes.

Alice's qubit is initially encoded onto a heralded single photon. Her PPLN waveguide is pumped directly to generate photon pairs, where the detection of one photon indicates the presence of a single photon in the other mode. After the waveguide, we use a 100-GHz 1300-nm dense wavelength division multiplexer (DWDM) as a notch filter for the pump, followed by a 1310-nm DWDM to separate each photon into different fibers via the DWDM's pass and reflect ports. The 1310-nm photon is filtered by a 10.5-GHz FWHM bandwidth fiber Bragg grating (FBG) filter and subsequently detected by a single photon detector. Due to energy conservation, this heralds a single photon with a center wavelength of 1290 nm. Alice's qubit is then encoded onto the horizontal (H) and vertical (V) components of the heralded photon's polarization $|\psi\rangle_A = \alpha|H\rangle + \beta|V\rangle$ using polarization waveplates. This photon is then multiplexed using a standard O-band/C-band WDM to co-propagate with the 400-Gbps C-band classical signal over 15.2 km of spooled optical fiber (SMF-28(R) ULL) to Charlie.

Bob's entangled photon pair source is designed similarly, except his PPLN waveguide is placed inside a polarization Sagnac loop to generate the two-photon quantum state $\frac{1}{\sqrt{2}}(|H_3H_i\rangle + e^{i\delta}|V_3V_i\rangle)$. Bob's 1290-nm photon is transmitted to counter-propagate with the 400-Gbps signal over 15.0 km of spooled fiber (SMF-28(R) ULL) to Charlie. However, Bob's 1310-nm photon is kept locally to act as the target photon for transferring Alice's state to Bob's node. This photon is sent to a free-space polarization module which first compensates rotations in the fibers and prepares the $|\Psi^-\rangle_B$ Bell state using alignment signals and coincidence detection [41], and then uses a quarter-waveplate, half-waveplate, and polarizing beam splitter (PBS) combination to allow for arbitrary projective measurements of the polarization of Bob's target photon. Subsequently, this photon is filtered by a 9.8-GHz FBG filter and then detected by a single-photon detector.

At Charlie's node, a BSM is performed on Alice and Bob's incident polarization qubits using conditional HOM interference at a 50:50 beam splitter [38]. Since HOM interference only occurs between identical photons, the fidelity of the BSM is governed by their spatial and spectro-temporal indistinguishability. To achieve this, a single-mode fiber 50:50 coupler is used for spatial indistinguishability and a variable optical delay in Alice's pump path is used to ensure that both photons arrive simultaneously at the coupler. Furthermore, the 1290-nm photons are filtered by 10.8-GHz FBGs. Together with the 1310-nm FBGs, this extends the photons' coherence times relative to the pump's and increases the probability that each photon is in a single identical spectral mode [42].

These narrow-band spectral filters also play a critical role in improving tolerance to classical power due to the SpRS noise photons being spectrally independent of the quantum signal. Another potential source of noise is residual C-band photons due to insufficient isolation when filtering the O-band quantum signals. This is prevented by placing two cascaded O-band/C-band WDMs before the FBGs and a 1290-nm DWDM, which altogether provides >190 dB isolation from C-band light.

To perform the BSM, we place two PBSs in each output arm of 50:50 coupler before the single photon detectors D_1 and D_2 , which are set to project onto the orthogonal polarization states $|H\rangle_{D_1}$ and $|V\rangle_{D_2}$. A two-fold coincidence detection at opposite ports of the 50:50 splitter indicates that Alice and Bob's photons were in the $|\Psi^-\rangle_{AB}$ Bell state due to HOM interference that oc-

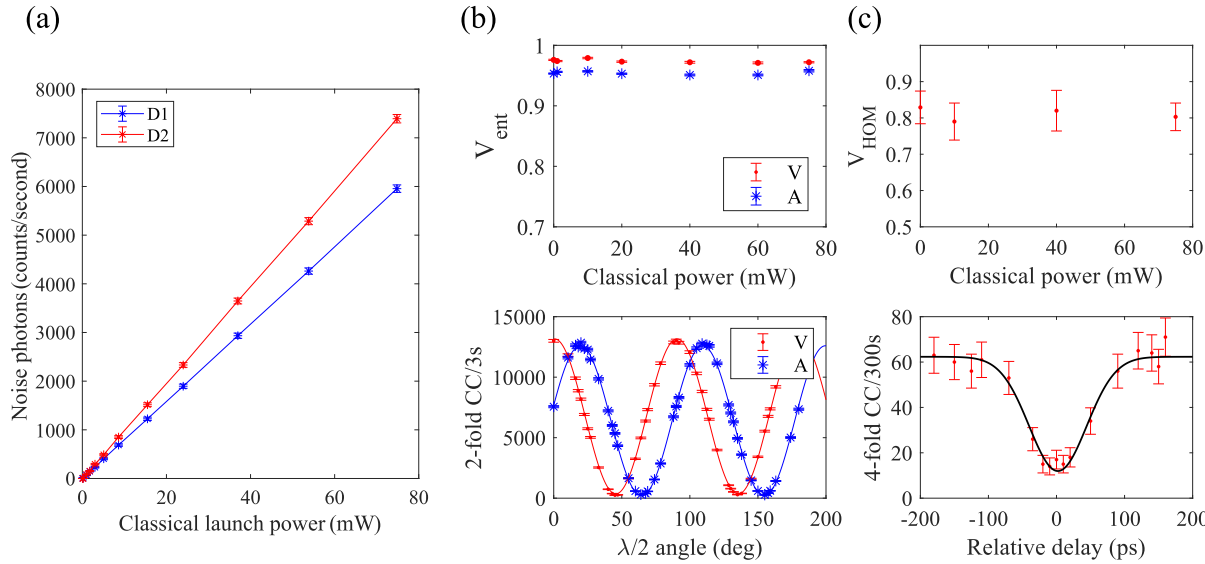


Fig. 2. (a) Noise photon single photon count rate in the Bell state measurement detectors D_1 and D_2 as a function of the 400-Gbps C-band signal's launch power P_{cl} injected into the 30.2-km fiber link. (b) Visibility of non-local two-photon interference fringes for Bob's entanglement distribution over 15.0 km to the Bell state measurement node as a function of P_{cl} (top) and the measured two-fold coincidence count (CC) interference fringes in the vertical (V) and anti-diagonal (A) bases for $P_{\text{cl}} = 74$ mW (bottom). (c) Hong-Ou-Mandel interference visibility between heralded photons from Alice and Bob as a function of P_{cl} (top) and an interference dip measurement when $P_{\text{cl}} = 74$ mW (bottom).

curse if they were in any of the three other Bell states [38]. Due to the non-local correlations of Bob's entangled state $|\Psi^-\rangle_B$, a successful BSM detection results in the target photon at Bob's node being equivalent to Alice's input state $|\psi\rangle_A$ [38]. We note that teleportation via detecting $|\Psi^-\rangle_{AB}$ can be performed without the PBSs. However, basis-selective Bell state analyzers are most common as they can double the success probability of a BSM by also measuring the $|\Psi^+\rangle$ Bell state, which could be done here if detectors were added to the other output ports of the PBSs [43]. Thus, this design allows us to evaluate how coexisting classical signals impact BSM nodes most likely to be implemented in future networks. We also note the PBSs at the BSM naturally filter SpRS noise in the polarization degree of freedom. Due to polarization mode dispersion, SpRS photons generated over long fibers are largely unpolarized [17, 44] which means polarizing elements can reduce noise rates by roughly a factor of two in each detector.

Teleportation is evaluated by measuring the polarization of Bob's target photon at detector D_3 conditioned on a three-fold coincidence detection between the heralding and BSM detectors, requiring four-fold coincidence detection. Photons are detected by superconducting nanowire single photon detectors (SNSPD), each having >90% detection efficiency and a dark count rate of ~100 counts/s. Photon arrival times are determined using a time-to-digital converter and coincidences are registered when the arrival times in each channel fall within a 500-ps wide time window. The coincidence logic can also be viewed as the classical channel in the teleportation protocol which informs Bob that a successful BSM occurred.

Since the modulation of the classical signal is uncorrelated with the pulsed quantum system, SpRS photons are randomly distributed in time relative to the quantum signals. As a result, narrow detection windows around the expected quantum signal arrival times act as a temporal filter on the noise. Furthermore,

the inherent temporal correlations in photon pair detection can provide another layer of timing information that can increase the signal-to-noise ratio compared to sources such as WCSs [45].

The quantum teleportation-classical coexistence study is conducted in a laboratory located at Northwestern University's Evanston campus. However, the classical transceiver is located in a building at the Northwestern University Chicago campus, which requires transmission over a 24-km deployed fiber pair to and from the Evanston location to operate. Thus, the classical signal travels an additional 48 km of fiber giving a total link distance of 78.2 km. The transmission loss over the 30.2-km fiber is 4.9 dB at the classical signal's 1547.32-nm wavelength and the 1290-nm quantum signals have a total loss of 10.1 dB (5.1 dB and 5.0 dB for Alice and Bob's photons, respectively). At Charlie, the bypassing of the BSM by the classical signal using WDMs adds an additional 1.2 dB insertion loss.

The total loss when transmitting the classical signal over the full 78.2-km fiber is 22.8 dB. Due to a receiver sensitivity of -18 dBm, the transceiver's output power of -9 dBm requires amplification for the system to operate error-free. To achieve this, we place two cascaded erbium doped fiber amplifiers (EDFA) at the Evanston location just before multiplexing into the 30.2-km link to co-propagate with Alice's photon. The minimum power launched into the 30.2-km fiber to achieve error-free communications could be as low as -3 dBm (0.5 mW) for the receiver located 30.2 km + 24 km away from the EDFA, and -10.7 dBm (85 μ W) if the receiver were instead located directly at the end of the 30.2-km link. However, in this study we explore elevated launch powers to emulate more hostile environments that could be encountered in the field such as those found in high-capacity long-distance DWDM classical network systems.

3. EXPERIMENTAL RESULTS

A. Noise rates, entanglement distribution, and Hong-Ou-Mandel interference

We now evaluate the performance of our quantum system. First, we characterize how much noise is introduced into the detectors D_1 and D_2 as a function of the classical power P_{cl} that is multiplexed into the 30.2-km fiber. Fig. 2(a) shows the single photon count rates as we increase P_{cl} , where the SNSPD dark count rates have been subtracted. The extra noise scales linearly with power as 79.0 counts/s/mW and 97.9 counts/s/mW in D_1 and D_2 , respectively, which differ due to slightly different detection system efficiencies. These results demonstrate that SpRS noise is significantly suppressed, as even mW power levels introduce extraneous noise on the order of the SNSPD dark count level. Since the 400-Gbps system can operate at $P_{\text{cl}} > 0.5$ mW, this means that the SNSPDs hardly notice any rise in background counts when the system is operating at the minimum necessary classical power.

As teleportation requires quantum entanglement as a resource and the ability to have indistinguishable photons for the BSM, we independently characterize the quality of Bob's entanglement distribution to Charlie and HOM interference as we vary P_{cl} . We set Alice and Bob's mean photon pairs per pulse and polarization qubit μ generated inside each PPLN waveguide to approximately $\mu_A = 0.018$ and $\mu_B = 0.013$, respectively, which are chosen to balance rates with reduced performance due to multi-pair emission during SPDC [46].

Fig. 2(b) shows how Bob's entanglement source's non-local two-photon interference fringe visibility in the vertical and anti-diagonal bases is impacted after distributing one photon over 15.0 km to Charlie as we increase the classical power launched into the full 30.2-km link. The visibility is defined as $V_{\text{ent}} = (R_{\text{max}} - R_{\text{min}})/(R_{\text{max}} + R_{\text{min}})$, where $R_{\text{max(min)}}$ are the maximum (minimum) two-fold coincidence counts of the interference fringe. Fig. 2(b) shows no noticeable degradation of V_{ent} up to $P_{\text{cl}} = 74$ mW, in which we measure visibilities of $V_V = 97.5 \pm 0.1\%$ and $V_A = 95.3 \pm 0.2\%$. All error bars in this paper are determined via the Monte-Carlo method assuming Poisson photon counting statistics. These results indicate that entanglement distribution is well preserved at high classical powers, and that visibility is mainly limited from unity due to multi-pair emission during SPDC. These values are also well above the $1/\sqrt{2}$ bound for demonstrating the non-local nature of quantum entanglement [47]. Thus, this state is more than sufficient to use as a resource for quantum teleportation.

Next, we characterize HOM interference between heralded photons from Alice and Bob's sources as we increase P_{cl} . To ensure polarization indistinguishably, we align the PBSs in the BSM setup to instead project onto $|H\rangle_{D_1}|H\rangle_{D_2}$ and prepare Alice and Bob's heralded photons in the state $|H\rangle$. We then record four-fold coincidences as we vary the relative time-of-arrival of each photon using Alice's variable optical delay. The quality of the interference is determined by the visibility of the fringe $V_{\text{HOM}} = (R_{\text{max}} - R_{\text{min}})/R_{\text{max}}$, where $R_{\text{max(min)}}$ are the maximum (minimum) four-fold coincidence rates of the HOM interference fringe. The results are shown in Fig. 2(c). We measure a visibility of $V_{\text{HOM}} = (R_{\text{max}} - R_{\text{min}})/R_{\text{max}} = 82.9 \pm 4.5\%$ without the classical source, which is comparable to the $V_{\text{HOM}} = 83.1 \pm 1.4\%$ visibility we obtain without distribution over the 30.2-km fiber. We measure $V_{\text{HOM}} = 80.3 \pm 3.8\%$ with P_{cl} set to 74 mW, showing interference is not significantly degraded by high-power coexisting C-band light. Each visibility

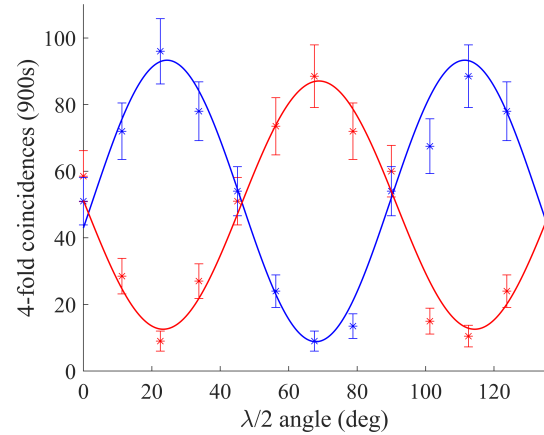


Fig. 3. Four-fold coincidence counts as we scan Bob's polarization analyzer setting along the Bloch sphere for Alice transmitting $|D\rangle$ (blue) and $|A\rangle$ (red) when the launch power of the 400-Gbps classical signal into the 30.2-km fiber is set to 74 mW.

is well above the classical bound of 50% [48], indicating our photons are sufficiently indistinguishable for performing quantum teleportation.

B. Quantum teleportation coexisting with high-rate classical communications

Looking at the performance of entanglement distribution and HOM interference, we find that the key operations underlying quantum teleportation are well maintained at high C-band power levels. To demonstrate that this translates to the ability to perform noise-resilient teleportation, we evaluate the teleportation of various qubits while simultaneously transmitting 74 mW of C-band classical power.

Fig. 3 shows four-fold coincidence counts as we scan Bob's polarization analyzer setting along the Bloch sphere for Alice transmitting $|D\rangle = \frac{1}{\sqrt{2}}(|H\rangle + |V\rangle)$ and $|A\rangle = \frac{1}{\sqrt{2}}(|H\rangle - |V\rangle)$. The coincidences exhibit sinusoidal fringes that coincide with Alice's prepared qubit. We obtain fringe visibilities of $V_D = 81.3 \pm 5.4\%$ and $V_A = 74.7 \pm 4.7\%$, both values being above the $V > 1/3$ classical limit [49].

Next, we perform maximum likelihood quantum state tomography [50] on Bob's target photon to reconstruct the density matrix ρ_B of his quantum state conditioned on a BSM detection. Fig. 4 shows ρ_B for Alice transmitting the states $|H\rangle$, $|V\rangle$, $|D\rangle$, and $|A\rangle$. The fidelity of ρ_B to Alice's ideal qubit $|\psi\rangle_A$ is determined by calculating $F_\psi = \langle \psi_A | \rho_B | \psi_A \rangle$. State transfer in the H/V basis does not require HOM interference due to the projection onto $|H\rangle_{D_1}|V\rangle_{D_2}$ in the Bell state analyzer [51], where raw fidelity is mainly limited from unity due to multi-photon pair degradation. In this basis, we measure $F_H = 97.5 \pm 1.2\%$ and $F_V = 95.8 \pm 2.5\%$ for $|\psi\rangle_A = |H\rangle$ and $|V\rangle$, respectively. However, transferring coherent superpositions of $|H\rangle$ and $|V\rangle$ requires interference and thus exhibit more decoherence due to an imperfect spectro-temporal indistinguishability between Alice and Bob's photons. For Alice transmitting $|\psi\rangle_A = |D\rangle$ and $|A\rangle$, we obtain fidelities of $F_D = 87.5 \pm 3.9\%$ and $F_A = 85.5 \pm 3.7\%$, respectively. Knowing that SpRS noise rates are independent of Alice's prepared qubit, assuming symmetry of the equatorial states we calculate the average fidelity

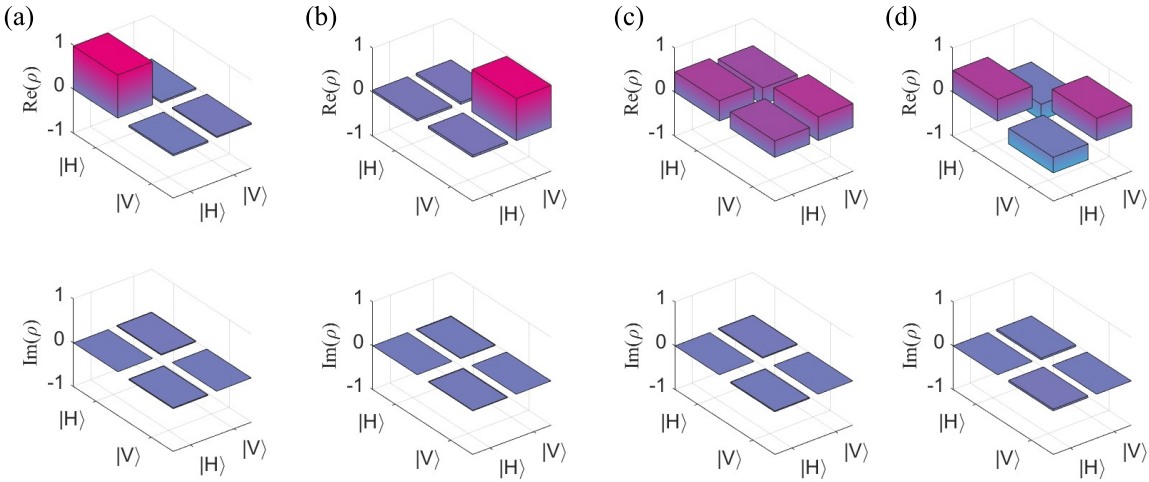


Fig. 4. Real and imaginary components of the density matrices obtained by single-qubit quantum state tomography on Bob’s target photon, conditioned on a successful BSM, whilst the launch power of the 400-Gbps C-band signal into the 30.2-km fiber is set to 74 mW. (a-d) show the results for Alice transmitting $|\psi\rangle_A = |H\rangle, |V\rangle, |D\rangle$, and $|A\rangle$, respectively.

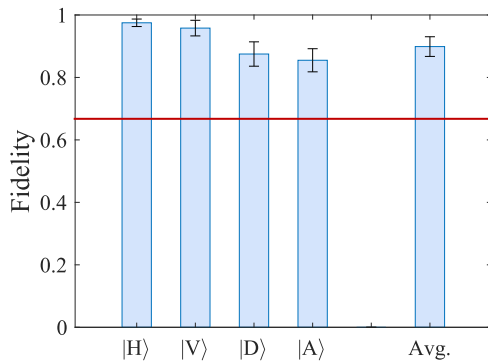


Fig. 5. Fidelity of the reconstructed density matrix of Bob’s state to Alice’s initially prepared state for four different qubits as well as the average fidelity when the power of the 400-Gbps classical signal is set to 74 mW. The horizontal line shows the $F > 2/3$ limit for demonstrating non-classical teleportation.

for an arbitrary qubit via $F_{\text{avg}} = (F_H + F_V + 2(F_D + F_A))/6$ in which we obtain $F_{\text{avg}} = 89.9 \pm 3.1\%$. Furthermore, we measure $F_{\text{avg}} = 90.4 \pm 2.7\%$ without sending the photons over the 30.2-km link, demonstrating that there is minimal degradation of fidelity from distribution over the fiber link nor the inclusion of the classical light. All of the measured fidelities are shown in Fig. 5. Since all are well above the classical bound of $F = 2/3$ [49], we have clearly demonstrated that non-classical teleportation can be performed alongside high-rate conventional classical communications.

4. DISCUSSION AND OUTLOOK

Since teleportation was conducted alongside much higher powers than necessary for the 400-Gbps classical system, this indicates that substantially higher data rates could have propagated through the fiber. The classical power used was 148 times greater than necessary for a single 400-Gbps channel, and 870

times greater than if the receiver were located directly at the end of the 30.2-km fiber. Thus, a multi-channel WDM classical system could easily have carried many terabits/s aggregate data rates without having a significant impact on quantum fidelity. The demonstrated powers are also on the order of the highest achieved in state-of-the-art single [10–12] and entangled [17] photon coexistence studies. This indicates the potential for teleportation-based quantum networking systems, such as quantum repeaters, operating alongside classical backbone networks [10].

Since our system uses two different photon pair sources, multiple nodes, and four-fold coincidence detection, our results indicate the potential for more complex systems operating alongside classical networks. For example, simple modifications to Alice’s source could allow entangled photon pair generation. A BSM at Charlie would then result in entanglement swapping [52], establishing entanglement between initially independent photons at Alice and Bob’s nodes. Due to our system’s high tolerance to classical power, it is reasonable to conclude that a similarly designed entanglement swapping system could operate alongside high-rate coexisting classical communications. Further, our multi-node configuration with the BSM performed near the midpoint of a longer fiber link is a key element for multi-node networking with a central quantum processor [34] and to implement quantum repeaters [29]. We note that these applications will also require quantum memories to store incident photons, the degree to which SpRS noise will impact various platforms and applications will require future investigation.

The state teleportation fidelity we obtained is comparable to recent experiments conducted over quantum-dedicated fiber networks [33, 34, 37], but could be further improved via standard methods. We showed that opposed to SpRS noise from coexisting classical light, our fidelity was mainly limited by multi-photon pair emission during SPDC and imperfect photon indistinguishability during the BSM. Raw fidelity could thus be improved by reducing the photon pair generation probability [46] and increasing indistinguishability by decreasing the ratio between the source’s pump spectral bandwidth to the photon filter bandwidths [42]. When considering SpRS noise, narrower

filters would simultaneously increase indistinguishability and reject more SpRS noise. Altogether, employing these approaches could allow our teleportation fidelity to approach more closely to unity and have an even higher tolerance to classical power.

Finally, classical signals are often used for quantum networking purposes. Some applications include communicating measurement results between nodes (eg., the BSM), synchronizing distant pulsed sources and detectors to a common clock, and channel monitoring. Similarly, quantum-classical coexistence can enhance functionality without sacrificing potentially limited fiber resources [16, 21, 22, 53]. Since these signals can typically operate well below the powers demonstrated here (sub-mW levels), our results show that including these signals in our system would have negligible impact if allocated to the C- or L-bands.

In conclusion, we have demonstrated a three-node quantum state teleportation system operating in a 30.2-km fiber link that simultaneously carries 400-Gbps conventional classical communications. By employing various methods to suppress the impact of SpRS noise photons, teleportation fidelity was well maintained with elevated classical powers capable of transmitting many terabits/s aggregate data rates. Since we have clearly shown that appropriately designed teleportation systems can operate alongside modern high-rate data traffic, this work demonstrates a significant step towards ensuring future quantum networking can be realized anywhere in the existing fiber infrastructure.

Funding. This work is funded by Subcontract No. 664603 from Fermi Research Alliance, LLC (FRA) to Northwestern University issued under Prime Contract No. DE-AC02-07CH11359 between FRA and the U.S. Department of Energy (DOE). Although the work is supported by the DOE's Advanced Scientific Computing Research Transparent Optical Quantum Networks for Distributed Science program, no government endorsement is implied.

Acknowledgments. The authors would like to acknowledge the support of StarLight International/National Communications Exchange Facility and Ciena Corporation. We further thank the members of the Advanced Quantum Networks for Scientific Discovery (AQNET-SD) project, which is a collaboration between Northwestern University, Caltech, Fermilab National Laboratory, Argonne National Laboratory, the Jet Propulsion Laboratory, and University of Illinois Urbana-Champaign towards advancing quantum network technology and applications.

Disclosures. The authors declare no conflicts of interest.

Data Availability Statement. Data may be obtained from the authors upon reasonable request.

REFERENCES

1. H. J. Kimble, "The quantum internet," *Nature* **453**, 1023–1030 (2008).
2. S. Wehner, D. Elkouss, and R. Hanson, "Quantum internet: A vision for the road ahead," *Science* **362**, eaam9288 (2018).
3. P. D. Townsend, "Simultaneous quantum cryptographic key distribution and conventional data transmission over installed fibre using wavelength-division multiplexing," *Electron. Lett.* **33**, 188–190(2) (1997). Publisher: Institution of Engineering and Technology.
4. T. E. Chapuran, P. Toliver, N. A. Peters, J. Jackel, M. S. Goodman, R. J. Runser, S. R. McNown, N. Dallmann, R. J. Hughes, K. P. McCabe, J. E. Nordholt, C. G. Peterson, K. T. Tyagi, L. Mercer, and H. Dardy, "Optical networking for quantum key distribution and quantum communications," *New J. Phys.* **11**, 105001 (2009).
5. P. Eraerds, N. Walenta, M. Legré, N. Gisin, and H. Zbinden, "Quantum key distribution and 1 Gbps data encryption over a single fibre," *New J. Phys.* **12**, 063027 (2010).
6. B. Qi, W. Zhu, L. Qian, and H.-K. Lo, "Feasibility of quantum key distribution through a dense wavelength division multiplexing network," *New J. Phys.* **12**, 103042 (2010).
7. K. A. Patel, J. F. Dynes, I. Choi, A. W. Sharpe, A. R. Dixon, Z. L. Yuan, R. V. Penty, and A. J. Shields, "Coexistence of High-Bit-Rate Quantum Key Distribution and Data on Optical Fiber," *Phys. Rev. X* **2**, 041010 (2012).
8. J. F. Dynes, W. W.-S. Tam, A. Plews, B. Fröhlich, A. W. Sharpe, M. Luccamarini, Z. Yuan, C. Radig, A. Straw, T. Edwards, and A. J. Shields, "Ultra-high bandwidth quantum secured data transmission," *Sci. Reports* **6**, 35149 (2016).
9. L.-J. Wang, K.-H. Zou, W. Sun, Y. Mao, Y.-X. Zhu, H.-L. Yin, Q. Chen, Y. Zhao, F. Zhang, T.-Y. Chen, and J.-W. Pan, "Long-distance copropagation of quantum key distribution and terabit classical optical data channels," *Phys. Rev. A* **95**, 012301 (2017).
10. Y. Mao, B.-X. Wang, C. Zhao, G. Wang, R. Wang, H. Wang, F. Zhou, J. Nie, Q. Chen, Y. Zhao, Q. Zhang, J. Zhang, T.-Y. Chen, and J.-W. Pan, "Integrating quantum key distribution with classical communications in backbone fiber network," *Opt. Express* **26**, 6010–6020 (2018).
11. J.-Q. Geng, G.-J. Fan-Yuan, S. Wang, Q.-F. Zhang, Y.-Y. Hu, W. Chen, Z.-Q. Yin, D.-Y. He, G.-C. Guo, and Z.-F. Han, "Coexistence of quantum key distribution and optical transport network based on standard single-mode fiber at high launch power," *Opt. Lett.* **46**, 2573–2576 (2021).
12. P. Gavignet, E. Pincemin, F. Herviou, Y. Loussouarn, F. Mondain, A. J. Grant, L. Johnson, R. I. Woodward, J. F. Dynes, B. Summers, A. J. Shields, K. Taira, H. Sato, R. Zink, V. Gremptka, V. Castay, and J. Zou, "Co-propagation of qkd & 6 tb/s (60x100g) dwdm channels with 17 dbm total wdm power in single and multi-span configurations," *J. Light. Technol.* pp. 1–7 (2023).
13. C. Liang, K. F. Lee, J. Chen, and P. Kumar, "Distribution of fiber-generated polarization entangled photon-pairs over 100 km of standard fiber in oc-192 wdm environment," in *2006 Optical Fiber Communication Conference and the National Fiber Optic Engineers Conference*, (2006), pp. 1–3.
14. A. Ciurana, V. Martin, J. Martinez-Mateo, B. Schrenk, M. Peev, and A. Poppe, "Entanglement Distribution in Optical Networks," *IEEE J. Sel. Top. Quantum Electron.* **21**, 37–48 (2015).
15. F. Hipp, M. Hentschel, S. Aleksic, A. Poppe, and H. Huebel, "Demonstration of a coexistence scheme between polarization-entangled QKD and classical data channels," in *Quantum Optics*, vol. 9900 J. Stuhler and A. J. Shields, eds., International Society for Optics and Photonics (SPIE, 2016), p. 99000P.
16. K. Kapoor, S. Xie, J. Chung, R. Valavarthi, C. Pena, L. Narvaez, N. Sinclair, J. P. Allmaras, A. D. Beyer, S. I. Davis, G. Fabre, G. Iskander, G. S. Kanter, R. Kettimuthu, B. Korzh, P. Kumar, N. Lauk, A. Mueller, M. Shaw, P. Spentzouris, M. Spiropulu, J. M. Thomas, and E. E. Wollman, "Picosecond Synchronization System for the Distribution of Photon Pairs through a Fiber Link between Fermilab and Argonne National Laboratories," *IEEE J. Quantum Electron.* pp. 1–1 (2023).
17. J. M. Thomas, G. S. Kanter, and P. Kumar, "Designing noise-robust quantum networks coexisting in the classical fiber infrastructure," *Opt. Express* **31**, 43035–43047 (2023).
18. Y.-R. Fan, Y. Luo, Z.-C. Zhang, Y.-B. Li, S. Liu, D. Wang, D.-C. Zhang, G.-W. Deng, Y. Wang, H.-Z. Song, Z. Wang, L.-X. You, C.-Z. Yuan, G.-C. Guo, and Q. Zhou, "Energy-time entanglement coexisting with fiber-optical communication in the telecom c band," *Phys. Rev. A* **108**, L020601 (2023).
19. X. Jing, C. Qian, X. Zheng, H. Nian, C. Wang, J. Tang, X. Gu, Y. Kong, T. Chen, Y. Liu, C. Sheng, D. Jiang, B. Niu, and L. Lu, "Coexistence of multiuser entanglement distribution and classical light in optical fiber network with a semiconductor chip," *Chip* p. 100083 (2024).
20. R. Wang, R. Yang, M. J. Clark, R. D. Oliveira, S. Bahrani, M. Peranić, M. Lončarić, M. Stipčević, J. Rarity, S. K. Joshi, S. K. Joshi, R. Nejabati, and D. Simeonidou, "Field trial of a dynamically switched quantum network supporting co-existence of entanglement, prepare-and-measure qkd and classical channels," in *49th European Conference on Optical Communications (ECOC 2023)*, (Institution of Engineering and Technology, 2023), p. 1682 – 1685.
21. S. J. B. Yoo, S. K. Singh, M. B. On, G. Gul, G. S. Kanter, R. Proietti, and P. Kumar, "Quantum wrapper networking," *IEEE Commun. Mag.* pp. 1–7 (2024).

22. A. Rahmouni, P. S. Kuo, Y. Li-Baboud, Y. S. I. A. Burenkov, M. V. Jabir, N. Lal, D. Reddy, M. Merzouki, L. Ma, A. Battou, S. V. Polyakov, O. Slattery, and T. Gerrits, "Metropolitan-scale entanglement distribution with coexisting quantum and classical signals in a single fiber," Arxiv (2024). ArXiv:2402.00617.

23. R. Valivarthy, P. Umesh, C. John, K. A. Owen, V. B. Verma, S. W. Nam, D. Oblak, Q. Zhou, and W. Tittel, "Measurement-device-independent quantum key distribution coexisting with classical communication," *Quantum Sci. Technol.* **4**, 045002 (2019).

24. R. C. Berrevoets, T. Middelburg, R. F. L. Vermeulen, L. D. Chiesa, F. Broggi, S. Piciaccia, R. Pluis, P. Umesh, J. F. Marques, W. Tittel, and J. A. Slater, "Deployed measurement-device independent quantum key distribution and Bell-state measurements coexisting with standard internet data and networking equipment," *Commun. Phys.* **5**, 186 (2022).

25. R. Kumar, H. Qin, and R. Alléaume, "Coexistence of continuous variable QKD with intense DWDM classical channels," *New J. Phys.* **17**, 043027 (2015).

26. J. C. Chapman, A. Miloshevsky, H.-H. Lu, N. Rao, M. Alshowkan, and N. A. Peters, "Two-mode squeezing over deployed fiber coexisting with conventional communications," *Opt. Express* **31**, 26254–26275 (2023).

27. C. H. Bennett, G. Brassard, C. Crépeau, R. Jozsa, A. Peres, and W. K. Wootters, "Teleporting an unknown quantum state via dual classical and einstein-podolsky-rosen channels," *Phys. Rev. Lett.* **70**, 1895–1899 (1993).

28. D. Collins, N. Gisin, and H. D. Riedmatten, "Quantum relays for long distance quantum cryptography," *J. Mod. Opt.* **52**, 735–753 (2005).

29. H.-J. Briegel, W. Dür, J. I. Cirac, and P. Zoller, "Quantum repeaters: The role of imperfect local operations in quantum communication," *Phys. Rev. Lett.* **81**, 5932–5935 (1998).

30. A. Serafini, S. Mancini, and S. Bose, "Distributed quantum computation via optical fibers," *Phys. Rev. Lett.* **96**, 010503 (2006).

31. X.-M. Hu, Y. Guo, B.-H. Liu, C.-F. Li, and G.-C. Guo, "Progress in quantum teleportation," *Nat. Rev. Phys.* **5**, 339–353 (2023).

32. O. Landry, J. A. W. van Houwelingen, A. Beveratos, H. Zbinden, and N. Gisin, "Quantum teleportation over the swisscom telecommunication network," *J. Opt. Soc. Am. B* **24**, 398–403 (2007).

33. R. Valivarthy, M. G. Puigibert, Q. Zhou, G. H. Aguilar, V. B. Verma, F. Marsili, M. D. Shaw, S. W. Nam, D. Oblak, and W. Tittel, "Quantum teleportation across a metropolitan fibre network," *Nat. Photonics* **10**, 676–680 (2016).

34. Q.-C. Sun, Y.-L. Mao, S.-J. Chen, W. Zhang, Y.-F. Jiang, Y.-B. Zhang, W.-J. Zhang, S. Miki, T. Yamashita, H. Terai, X. Jiang, T.-Y. Chen, L.-X. You, X.-F. Chen, Z. Wang, J.-Y. Fan, Q. Zhang, and J.-W. Pan, "Quantum teleportation with independent sources and prior entanglement distribution over a network," *Nat. Photonics* **10**, 671–675 (2016).

35. Q.-C. Sun, Y.-F. Jiang, Y.-L. Mao, L.-X. You, W. Zhang, W.-J. Zhang, X. Jiang, T.-Y. Chen, H. Li, Y.-D. Huang, X.-F. Chen, Z. Wang, J. Fan, Q. Zhang, and J.-W. Pan, "Entanglement swapping over 100 km optical fiber with independent entangled photon-pair sources," *Optica* **4**, 1214 (2017).

36. R. Valivarthy, S. I. Davis, C. Peña, S. Xie, N. Lauk, L. Narváez, J. P. Allmaras, A. D. Beyer, Y. Gim, M. Hussein, G. Iskander, H. L. Kim, B. Korzh, A. Mueller, M. Rominsky, M. Shaw, D. Tang, E. E. Wollman, C. Simon, P. Spentzouris, D. Oblak, N. Sinclair, and M. Spiropulu, "Teleportation systems toward a quantum internet," *PRX Quantum* **1**, 020317 (2020).

37. S. Shen, C. Yuan, Z. Zhang, H. Yu, R. Zhang, C. Yang, H. Li, Z. Wang, Y. Wang, G. Deng, H. Song, L. You, Y. Fan, G. Guo, and Q. Zhou, "Hertz-rate metropolitan quantum teleportation," *Light. Sci. & Appl.* **12**, 115 (2023).

38. S. L. Braunstein and A. Mann, "Measurement of the bell operator and quantum teleportation," *Phys. Rev. A* **51**, R1727–R1730 (1995).

39. C. K. Hong, Z. Y. Ou, and L. Mandel, "Measurement of subpicosecond time intervals between two photons by interference," *Phys. Rev. Lett.* **59**, 2044–2046 (1987).

40. S. Arahira, N. Namekata, T. Kishimoto, H. Yaegashi, and S. Inoue, "Generation of polarization entangled photon pairs at telecommunication wavelength using cascaded $\chi(2)$ processes in a periodically poled linbo3 ridge waveguide," *Opt. Express* **19**, 16032–16043 (2011).

41. S. X. Wang and G. S. Kanter, "Robust multiwavelength all-fiber source of polarization-entangled photons with built-in analyzer alignment signal," *IEEE J. Sel. Top. Quantum Electron.* **15**, 1733–1740 (2009).

42. J. G. Rarity, "Interference of single photons from separate sources," *Ann. New York Acad. Sci.* **755**, 624–631 (1995).

43. K. Mattle, H. Weinfurter, P. G. Kwiat, and A. Zeilinger, "Dense coding in experimental quantum communication," *Phys. Rev. Lett.* **76**, 4656–4659 (1996).

44. J. C. Chapman, J. M. Lukens, M. Alshowkan, N. Rao, B. T. Kirby, and N. A. Peters, "Coexistent quantum channel characterization using spectrally resolved bayesian quantum process tomography," *Phys. Rev. Appl.* **19**, 044026 (2023).

45. M. T. Liu and H. C. Lim, "Transmission of o-band wavelength-division-multiplexed heralded photons over a noise-corrupted optical fiber channel," *Opt. Express* **21**, 30358–30369 (2013).

46. M. Takeoka, R.-B. Jin, and M. Sasaki, "Full analysis of multi-photon pair effects in spontaneous parametric down conversion based photonic quantum information processing," *New J. Phys.* **17**, 043030 (2015).

47. J. F. Clauser, M. A. Horne, A. Shimony, and R. A. Holt, "Proposed Experiment to Test Local Hidden-Variable Theories," *Phys. Rev. Lett.* **23**, 880–884 (1969).

48. H. Paul, "Interference between independent photons," *Rev. Mod. Phys.* **58**, 209–231 (1986).

49. S. Massar and S. Popescu, "Optimal extraction of information from finite quantum ensembles," *Phys. Rev. Lett.* **74**, 1259–1263 (1995).

50. J. Altepeter, E. Jeffrey, and P. Kwiat, "Photonic state tomography," (Academic Press, 2005), pp. 105–159.

51. F. Basso Basset, F. Salusti, L. Schweickert, M. B. Rota, D. Tedeschi, S. F. Covre da Silva, E. Roccia, V. Zwiller, K. D. Jöns, A. Rastelli, and R. Trotta, "Quantum teleportation with imperfect quantum dots," *npj Quantum Inf.* **7**, 7 (2021).

52. M. Żukowski, A. Zeilinger, M. A. Horne, and A. K. Ekert, "event-ready-detectors" bell experiment via entanglement swapping," *Phys. Rev. Lett.* **71**, 4287–4290 (1993).

53. I. A. Burenkov, A. Semionov, Hala, T. Gerrits, A. Rahmouni, D. Anand, Y.-S. Li-Baboud, O. Slattery, A. Battou, and S. V. Polyakov, "Synchronization and coexistence in quantum networks," *Opt. Express* **31**, 11431–11446 (2023).